Electronic Supplementary Material (ESI) for Energy Advances.

Enhanced Uranium Extraction Selectivity from Seawater Using Dopant Engineered Layered Double Hydroxides (Supporting Information)

Muhammad Zubair [a], Hayden Ou [a], Yuwei Yang [a], Daniel T. Oldfield [b], Lars Thomsen [c], Bijil Subhash [a], Jessica L. Hamilton [c], Joshua T. Wright [d], Nicholas M. Bedford [a], Jessica Veliscek-Carolan [b]**

[a] School of Chemical Engineering, The University of New South Wales, Sydney, NSW 2052, Australia
[b] ANSTO, Locked Bag 2001, Kirrawee DC, NSW 2232, Australia
[c] Australian Synchrotron, ANSTO, 800 Blackburn Road, Clayton, VIC 3168, Australia
[d] Department of Physics, Illinois Institute of Technology, Chicago, IL 60616, United States of America
* Corresponding authors

Table of Contents

Composition of Simulated Seawater Solution	2
Preparation of LDH materials for X-ray Absorption Spectroscopy (XAS)	2
Elemental Analysis	2
X-ray Diffraction	3
Fourier Transform Infra-Red Spectroscopy (FTIR)	3
Scanning Electron Microscopy	4
Nitrogen Porosimetry	7
X-ray Absorption Near Edge Structure (XANES) of as-made LDH	8
Adsorption Capacity	9
Adsorption Kinetics	9
Chemical Stability	9
Extended X-ray Absorption Fine Structure (EXAFS)	10
Wavelet transformation (WT) analysis	11
EXAFS modelling Fits	14
Near Edge X-ray Absorption Fine Structure (NEXAFS)	17
SEM after U sorption	18
References	19

Simulated Seawater

Table S1: Composition of Simulated Seawater Solution.

Ion	Metal Concentration	Compound
Na^{+}	3.5 wt%	NaCl
Mg^{+}	1300 mg/L	$MgCl_2.6H_2O$
Ca^{2+}	400 mg/L	$CaCl_2.2H_2O$
K^{+}	400 mg/L	K_2CO_3
V^{5+}	1 mg/L	NH_4VO_3
U^{6+}	1 mg/L	-

Seawater collection location and conditions
Location: Coogee Beach, Sydney, NSW, Australia
GPS: 33.9203° S, 151.2581° E
Average Temperature (October 2021): 19°C
Salinity: 36 % (g/L) (From NOAA ocean atlas)

Preparation of LDH materials for X-ray Absorption Spectroscopy (XAS)

The amount of U loaded into the LDH materials (mg/g), as well as the amount of Mg, Al and dopant elements lost from the LDH materials during U sorption, are reported in Table S1.

Table S2: U loading and Mg/Al/dopant loss of LDH samples for EXAFS and NEXAFS measurements

Sample	U loaded (mg/g)	Mg loss (%)	Al loss (%)	dopant loss (%)
MgAl	10.5 ± 0.1	16	1	
MgAlFe	10.4 ± 0.1	14	1	1
MgAlCe	11.1 ± 0.1	16	1	0
MgAlNd	9.9 ± 0.2	18	1	1
MgAlEu	5.1 ± 0.1	10	2	2
MgAlTb	4.2 ± 0.1	5	0	0

Elemental Analysis

Table S3: Elemental analysis of digested LDH samples and resulting chemical compositions

	weight%				chemical composition
	Na	Mg	Al	dopant	
MgAl	3.2 ± 0.04	25.6 ± 0.1	7.1 ± 0.02		$Mg_{0.8}Al_{0.2}(OH)_2(NO_3)_{0.2}.(NaNO_3)_{0.11}$
MgAlFe	4.2 ± 0.01	18.0 ± 0.1	6.4 ± 0.1	4.8 ± 0.04	$Mg_{0.70}Al_{0.22}Fe_{0.08}(OH)_2(NO_3)_{0.30}.(NaNO_3)_{0.17}$
MgAlCe	4.9 ± 0.01	15.9 ± 0.04	5.2 ± 0.03	9.5 ± 0.04	$Mg_{0.72}Al_{0.21}Ce_{0.07}(OH)_2(NO_3)_{0.28}.(NaNO_3)_{0.23}$
MgAlNd	5.1 ± 0.003	16.6 ± 0.03	5.4 ± 0.02	9.4 ± 0.02	$Mg_{0.72}Al_{0.21}Nd_{0.07}(OH)_2(NO_3)_{0.28}.(NaNO_3)_{0.23}$
MgAlEu	5.1 ± 0.1	16.4 ± 0.1	5.6 ± 0.1	9.5 ± 0.1	$Mg_{0.71}Al_{0.22}Eu_{0.07}(OH)_2(NO_3)_{0.29}.(NaNO_3)_{0.24}$
MgAlTb	5.2 ± 0.1	16.0 ± 0.2	4.9 ± 0.1	7.2 ± 0.1	$Mg_{0.74}Al_{0.21}Tb_{0.05}(OH)_2(NO_3)_{0.26}.(NaNO_3)_{0.26}$

X-ray Diffraction

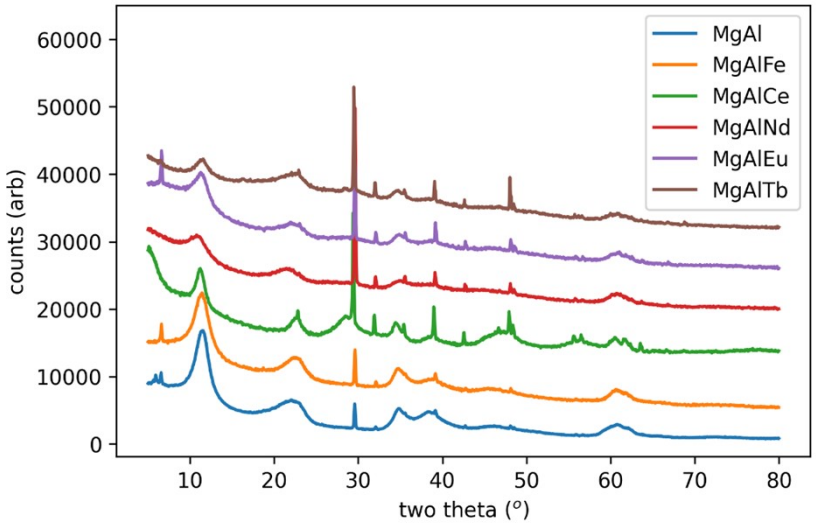

Figure S1: XRD patterns of as-made LDH samples.

Fourier Transform Infra-Red Spectroscopy (FTIR)

The FTIR-ATR spectra from 600 to 4000 cm^{-1} of all LDHs are shown in Figure S2. The predominant absorbance band at 1350 cm^{-1} and the smaller peak at 835 cm^{-1} are attributed to the antisymmetric and symmetric stretch vibrations of the interlayer nitrate anion,[1] as seen in previously synthesised LDH materials.[2,3] Further, the absorbance bands at 1620 cm^{-1} is due to the bending vibrations of water molecules in the interlayers. The characteristic band ~3400 cm^{-1} was attributed to the OH stretching mode of M-OH layer and the shoulder peak ~3550 cm^{-1} was assigned to stretching of interlayer water molecules. The absorbance bands below 800 cm^{-1} are assigned to stretching of Mg-O(H) and Al-O(H).[3,4]

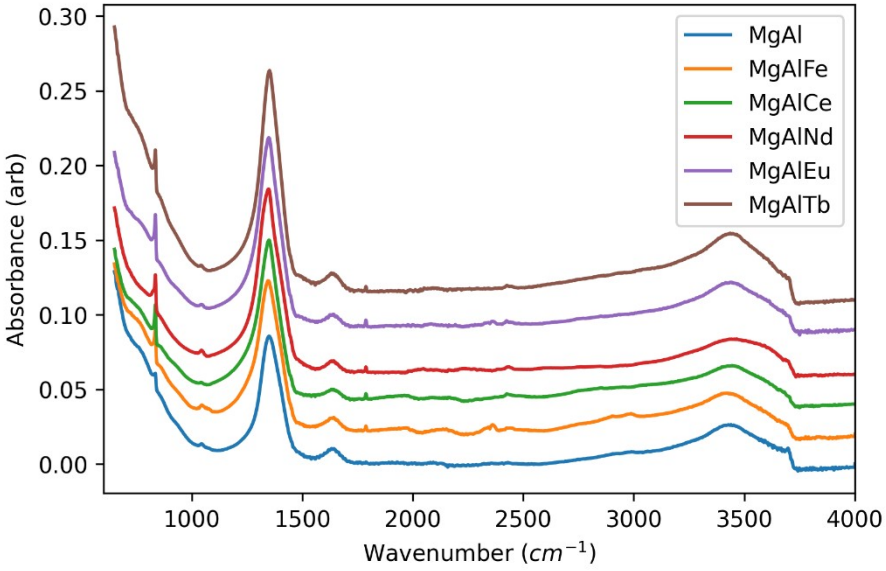

Figure S2: FTIR-ATR spectra of all LDH samples

Scanning Electron Microscopy

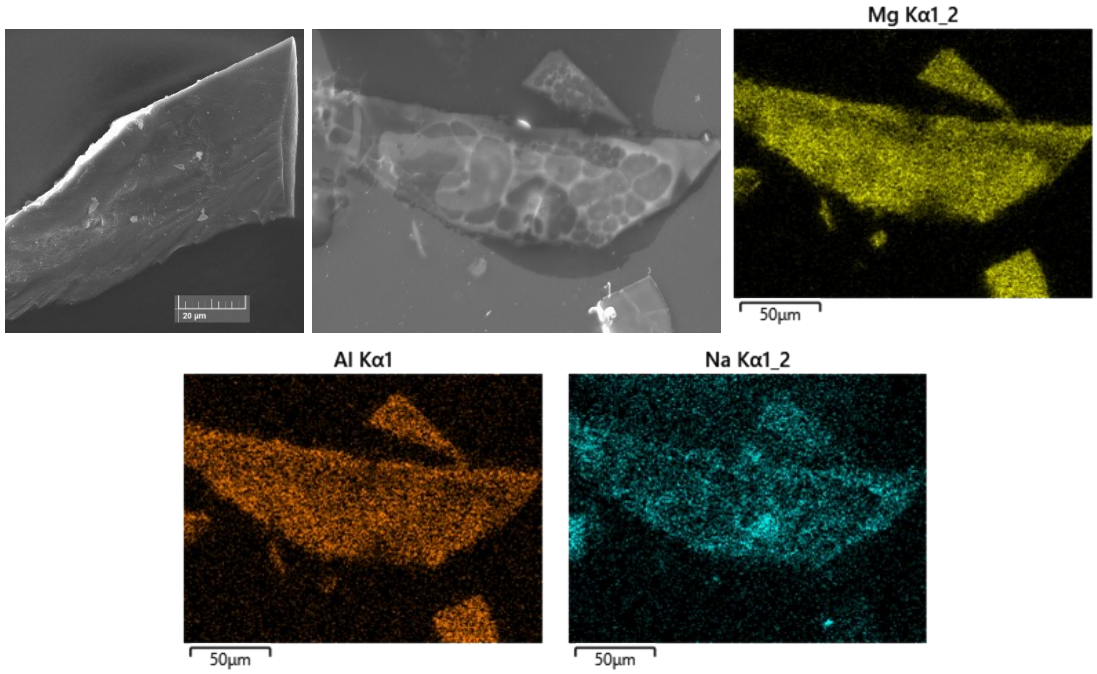

Figure S3: SEM/EDS images of MgAl LDH

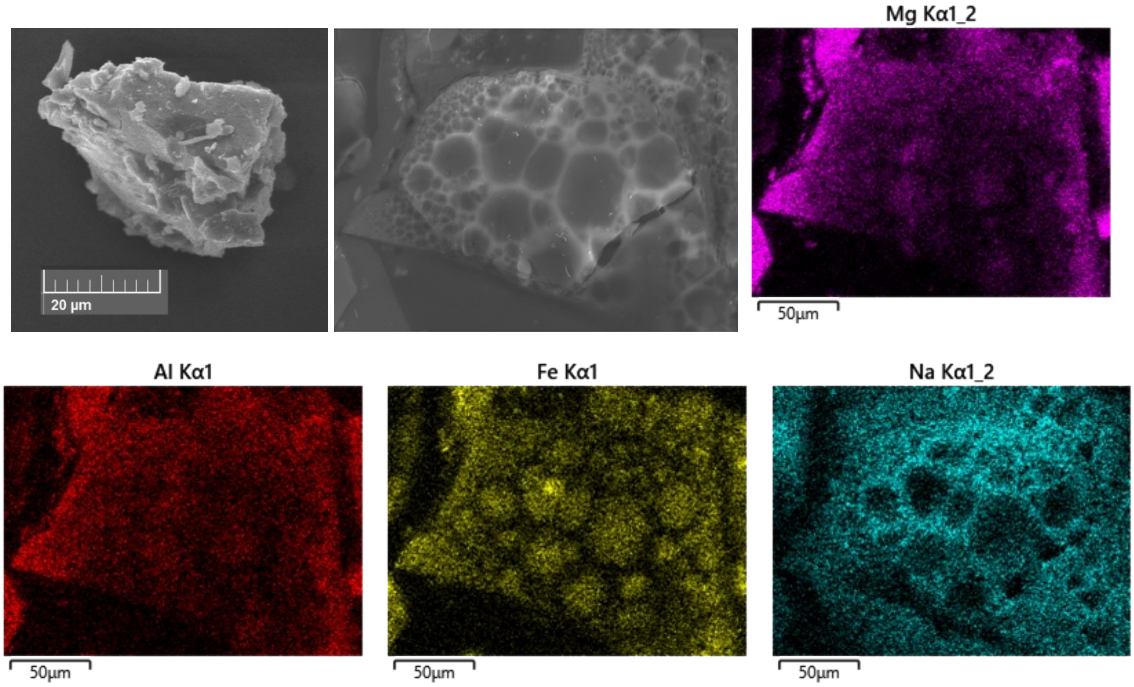

Figure S4: SEM/EDS images of MgAlFe LDH

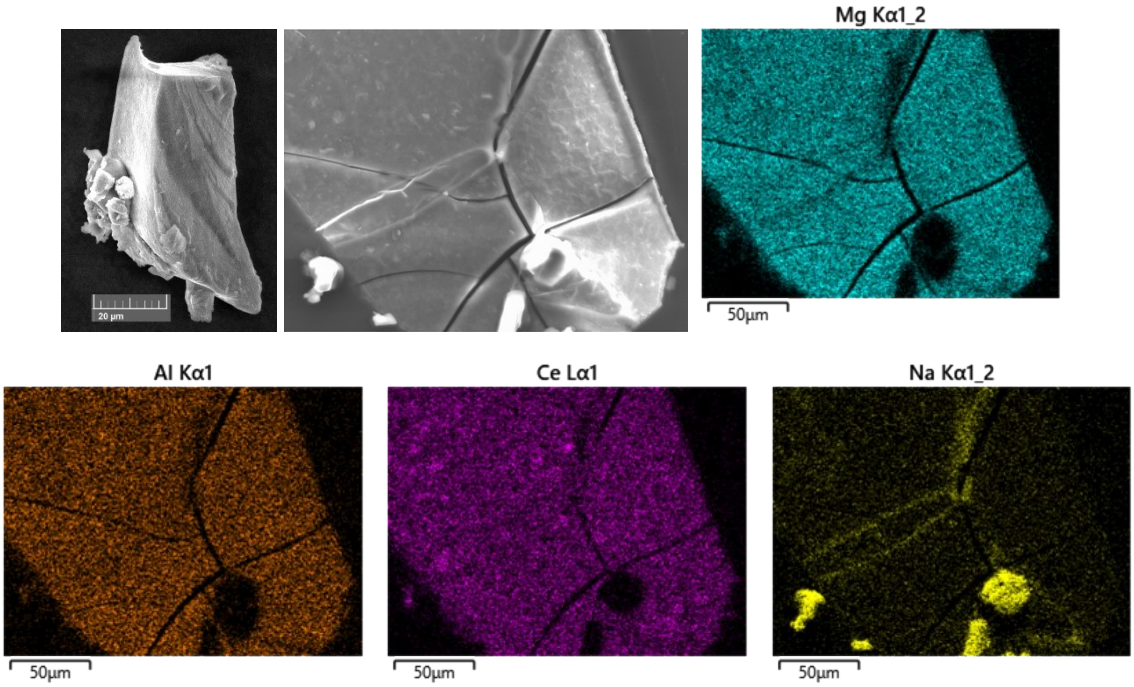

Figure S5: SEM/EDS images of MgAlCe LDH

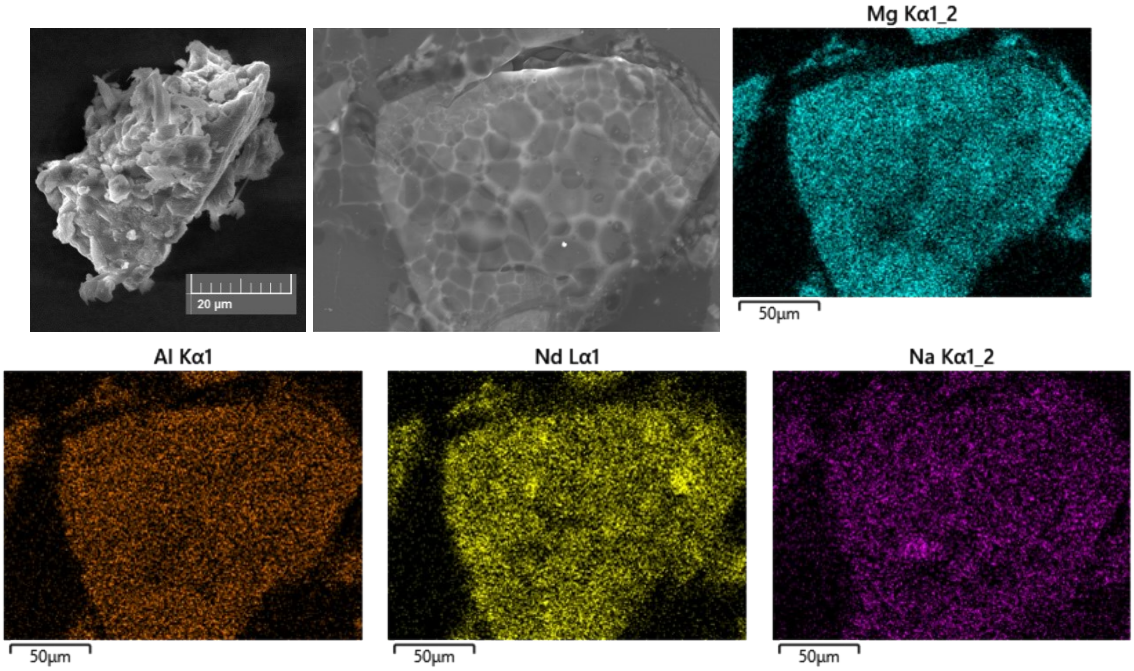

Figure S6: SEM/EDS images of MgAlNd LDH

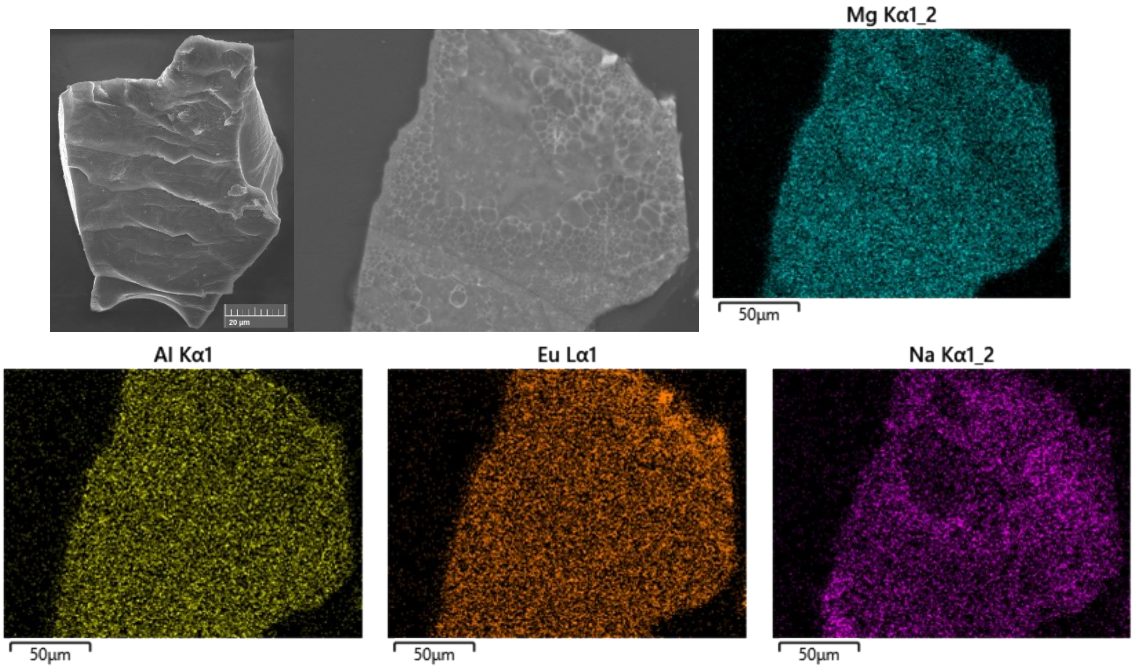

Figure S7: SEM/EDS images of MgAlEu LDH

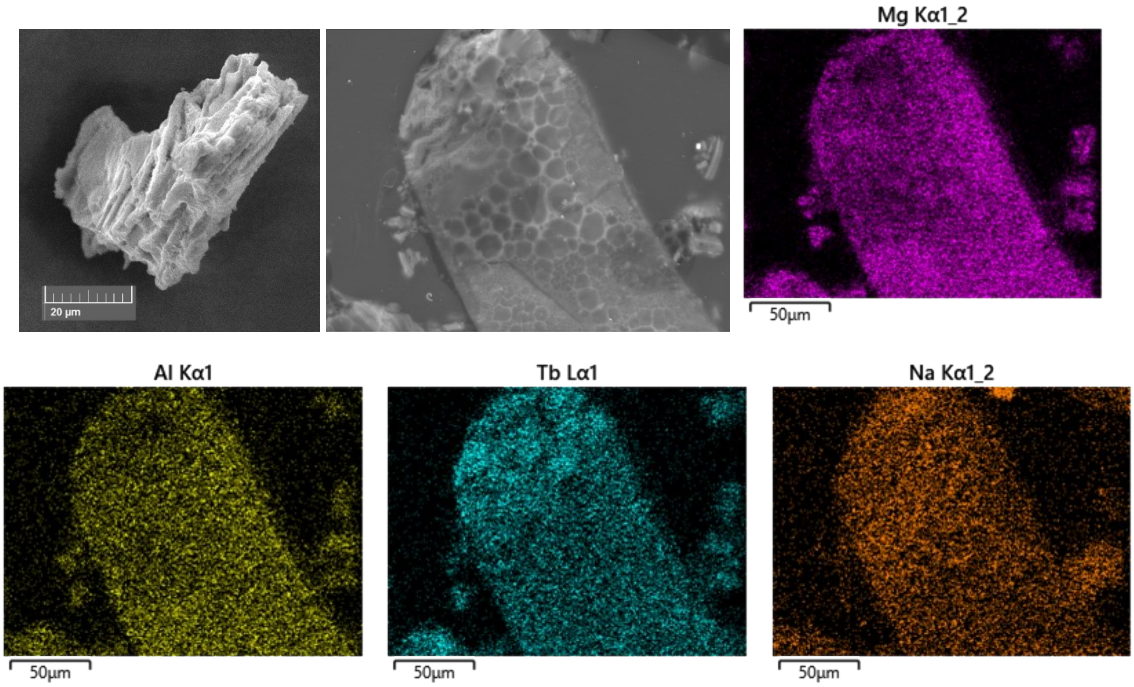

Figure S8: SEM/EDS images of MgAlTb LDH

Nitrogen Porosimetry

The physicochemical properties of as-made LDH samples, measured via nitrogen porosimetry, are given in Table S4. Pore size was predominantly 5-10 nm for MgAlCe and MgAlNd, while larger mesopores with diameter 15-18 nm were present in MgAlTb and MgAlEu showed a broad pore size distribution from mesopores to macropores. Pore sizes ranging from 5-13 nm have been reported for previously synthesised MgAl LDHs,[5,6] consistent with the results in Table S3.

Table S4: Physicochemical properties of LDH samples

Sample	BET surface area (m^2/g)	Pore Volume (mL/g)	Pore size (nm)
MgAl	0.4	0.01	6.2
MgAlFe	6.0	0.05	6.6
MgAlCe	15.1	0.07	6.7
MgAlNd	37.7	0.16	8.0
MgAlEu	25.7	0.20	15.6
MgAlTb	17.4	0.12	14.8

The nitrogen adsorption-desorption isotherms of MgAlCe, MgAlNd and MgAlTb (Figure S9) were all Type IV with H2/H3 hysteresis, indicating the presence of mesopores in these samples.[7] In contrast, MgAlEu produced a Type III isotherm shape and showed some low pressure hysteresis, suggesting this sample was macroporous and may have undergone swelling during the nitrogen adsorption process.

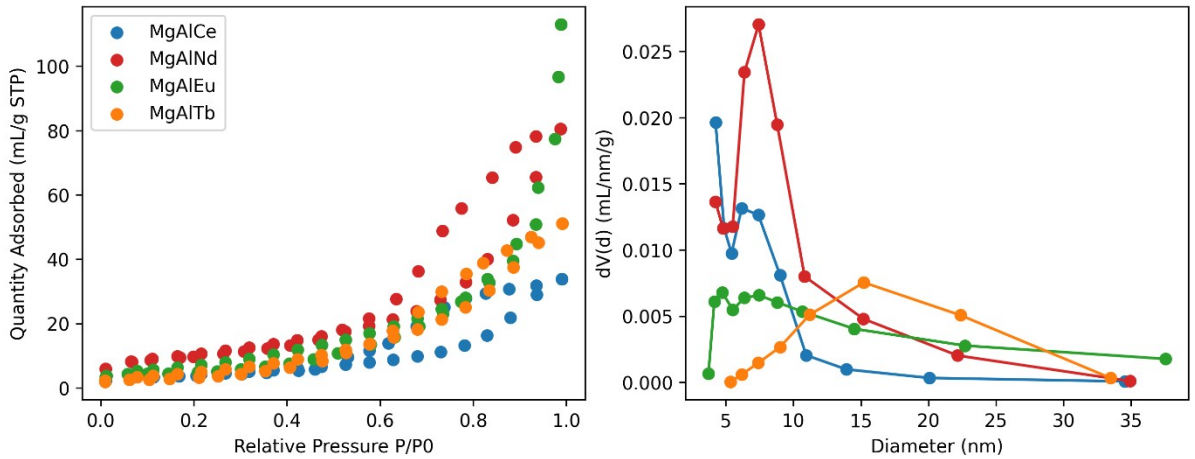

Figure S9: Nitrogen adsorption-desorption isotherms (left) and pore size distributions (right) for LDH samples with BET surface area greater than 10 m^2/g.

X-ray Absorption Near Edge Structure (XANES) of as-made LDH

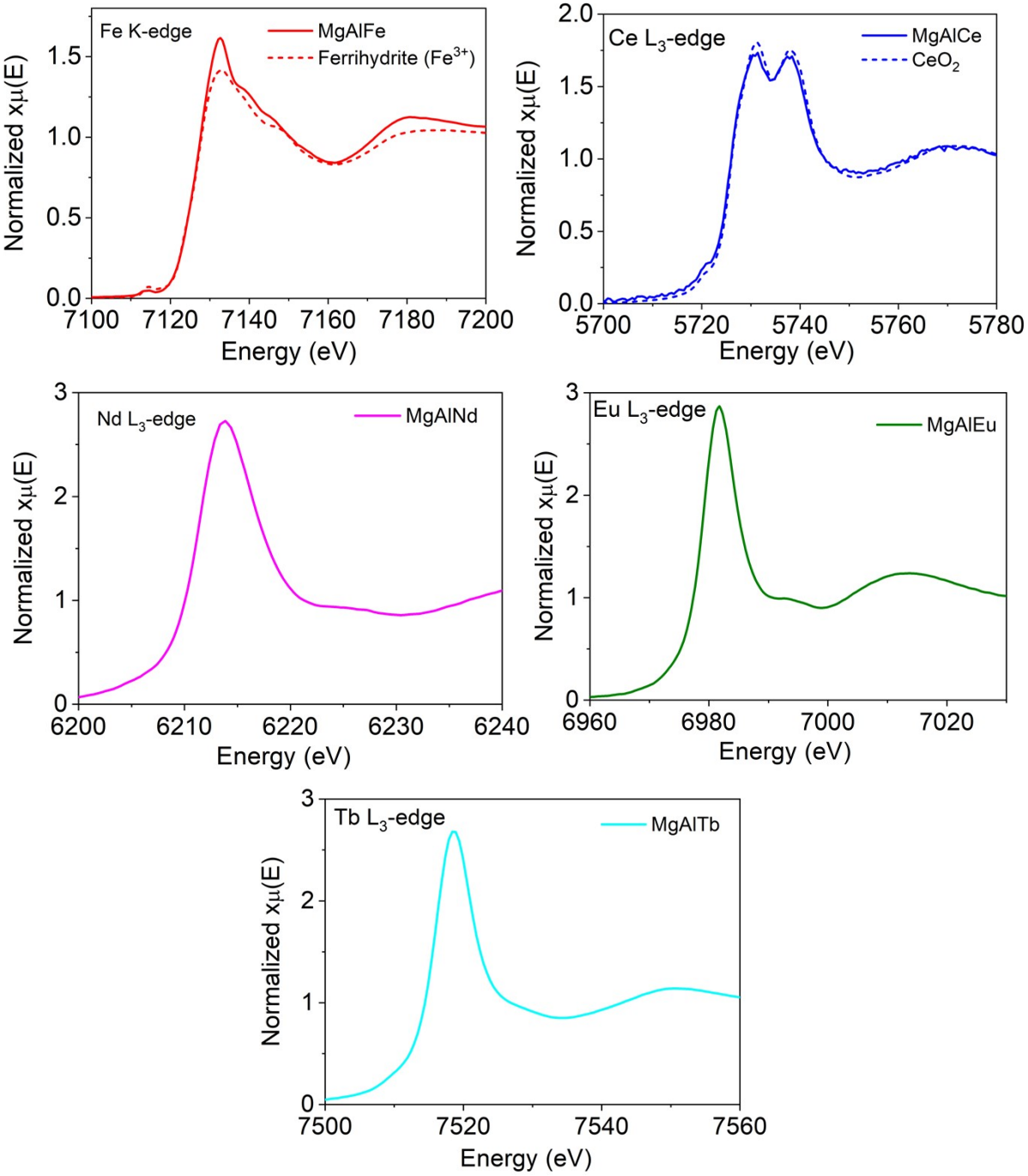

Figure S10: XANES of dopant elements in as-made LDH samples.

Adsorption Capacity

Table S5: Model isotherm constants for MgAl and MgAlNd.

Model		MgAl	MgAlNd
Langmuir	C_m (mg/g)	54.8	8.6
	b	1.29	4.48
	RSS	*30.6*	*4.62*
Freundlich	b	25.0	6.51
	n	0.48	0.29
	RSS	*14.3*	*0.48*

Adsorption Kinetics

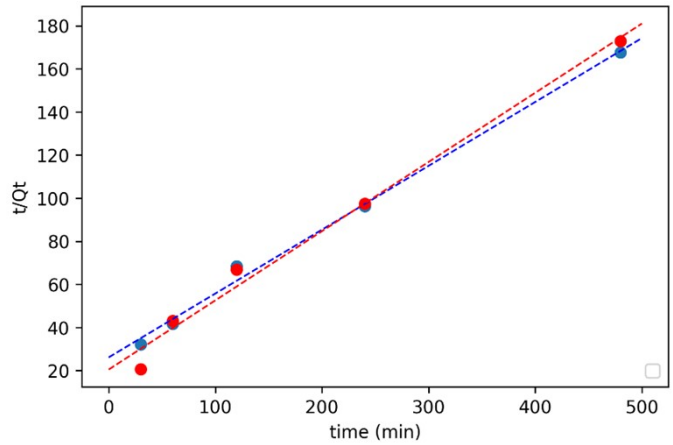

Figure S11: Pseudo second order kinetics fit for MgAl and MgAlNd with 3 ppm U in pH 8 Na_2CO_3 and V/m 1000.

Chemical Stability

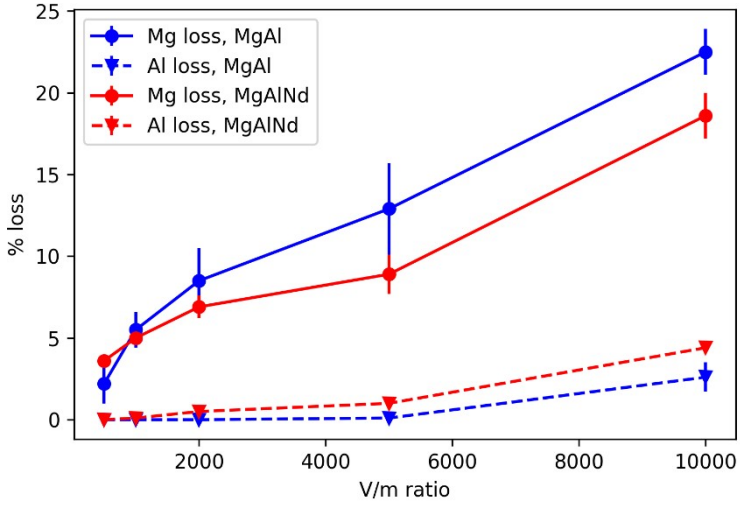

Figure S12: Percentage loss of Mg and Al from MgAl and MgAlNd LDH samples during capacity measurements. Loss of Nd was <1% for all V/m ratios.

Extended X-ray Absorption Fine Structure (EXAFS)

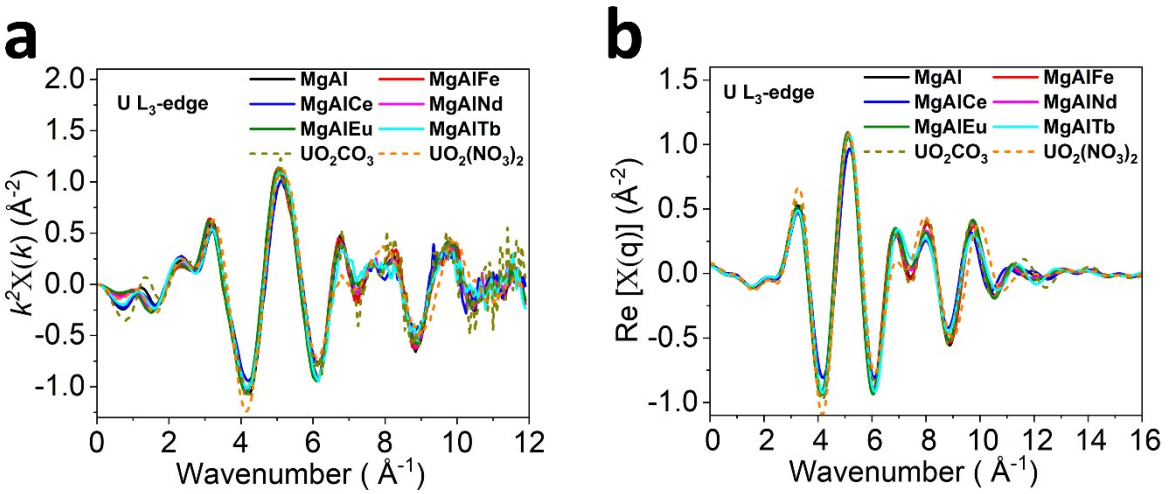

Figure S13: U-L3 Edge EXAFS (a) EXAFS oscillations in k space (k_2-weighting) (b) Real part of Fourier-filtered k-space

Wavelet Transformation

The wavelet transformation (WT) can be used as an efficient tool to interpret the extended X-ray absorption fine structure (EXAFS) spectra. The WT analysis provides direct visualization in three-dimension: the interatomic distance (R), the wavevector (k), and the WT modulus (the amplitude terms). This information is particularly important to perform nearest-neighbours analysis in the EXAFS.[8] We used Continuous Cauchy Wavelet Transformation (CCWT) to do the analysis. The resolution in k and R space can be controlled by the Cauchy parameter, **n** through the following equations:

$$[k - \Delta k\ , k + \Delta k\ ] \times \left[R + \Delta R_1\ , R + \Delta R_2\ \right] \tag{1}$$

while

$$\Delta k = \frac{1}{R}\left(\frac{n}{2\sqrt{2n-1}}\right) \tag{2}$$

and

$$\Delta R_1 = R\left(\frac{1}{2n} - \frac{\sqrt{2n+1}}{2n}\right);\ \Delta R_2 = R\left(\frac{1}{2n} + \frac{\sqrt{2n+1}}{2n}\right) \tag{3}$$

Further, Δk and ΔR are restricted by the Heisenberg uncertainty: ΔkΔR ≥ 1/4.[9] The value of **n** determines the resolution as Δk and ΔR are inversely proportional to each other. In present study, WTs were calculated with n = 200, such that for R values around 2 Å, the resolutions in the k and R spaces are, respectively, ΔR ± 0.1 Å and Δk ± 2.5 $Å^{-1}$

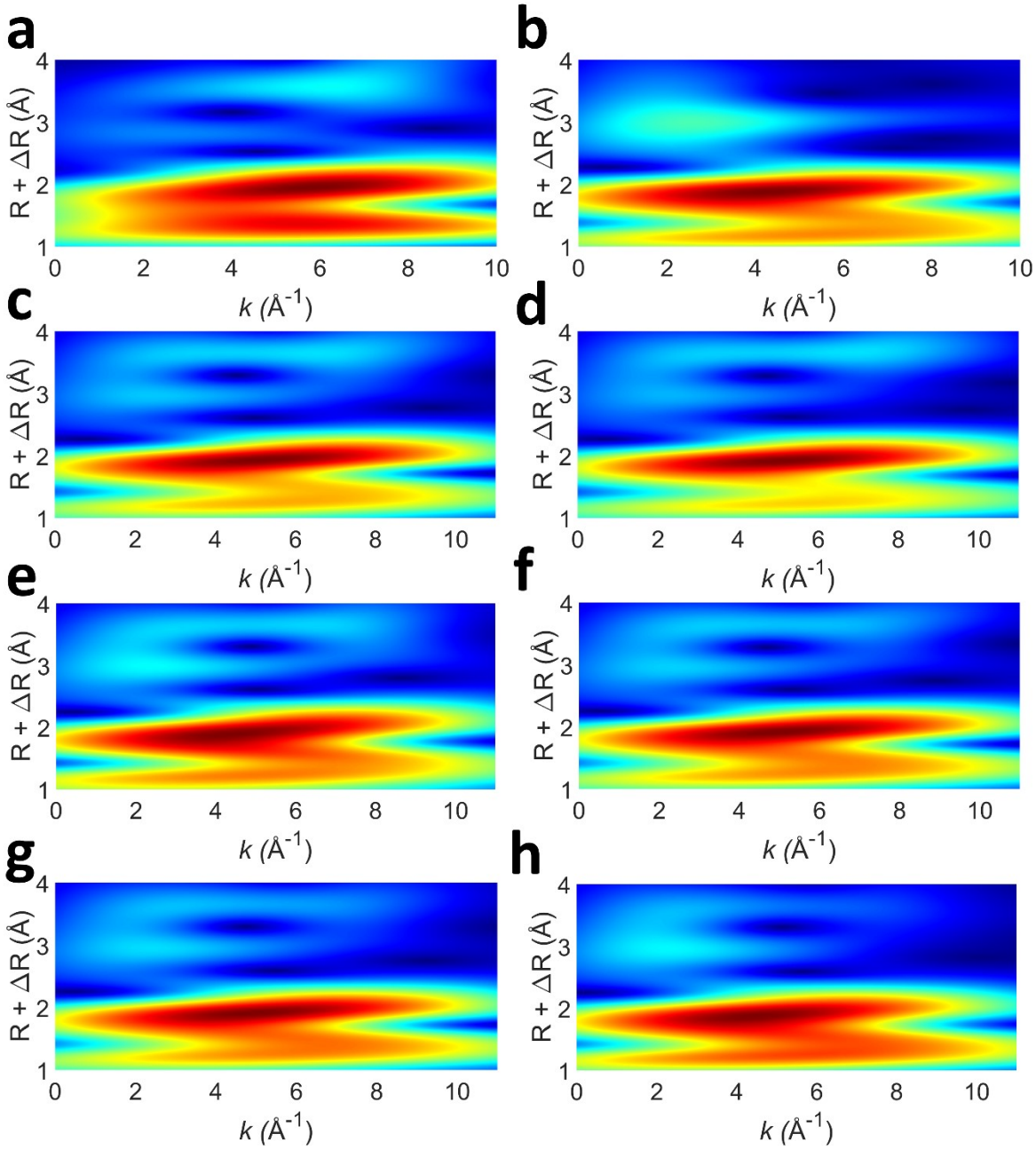

Figure S14: U-L_3 Edge EXAFS WT analysis (1-4 Å and k_2= 0-10) for (a) UO_2CO_3 standard (b) $UO_2(NO_3)_2$ standard (c) MgAl (d) MgAlFe (e) MgAlCe (f) MgAlNd (g) MgAlEu (h) MgAlTb

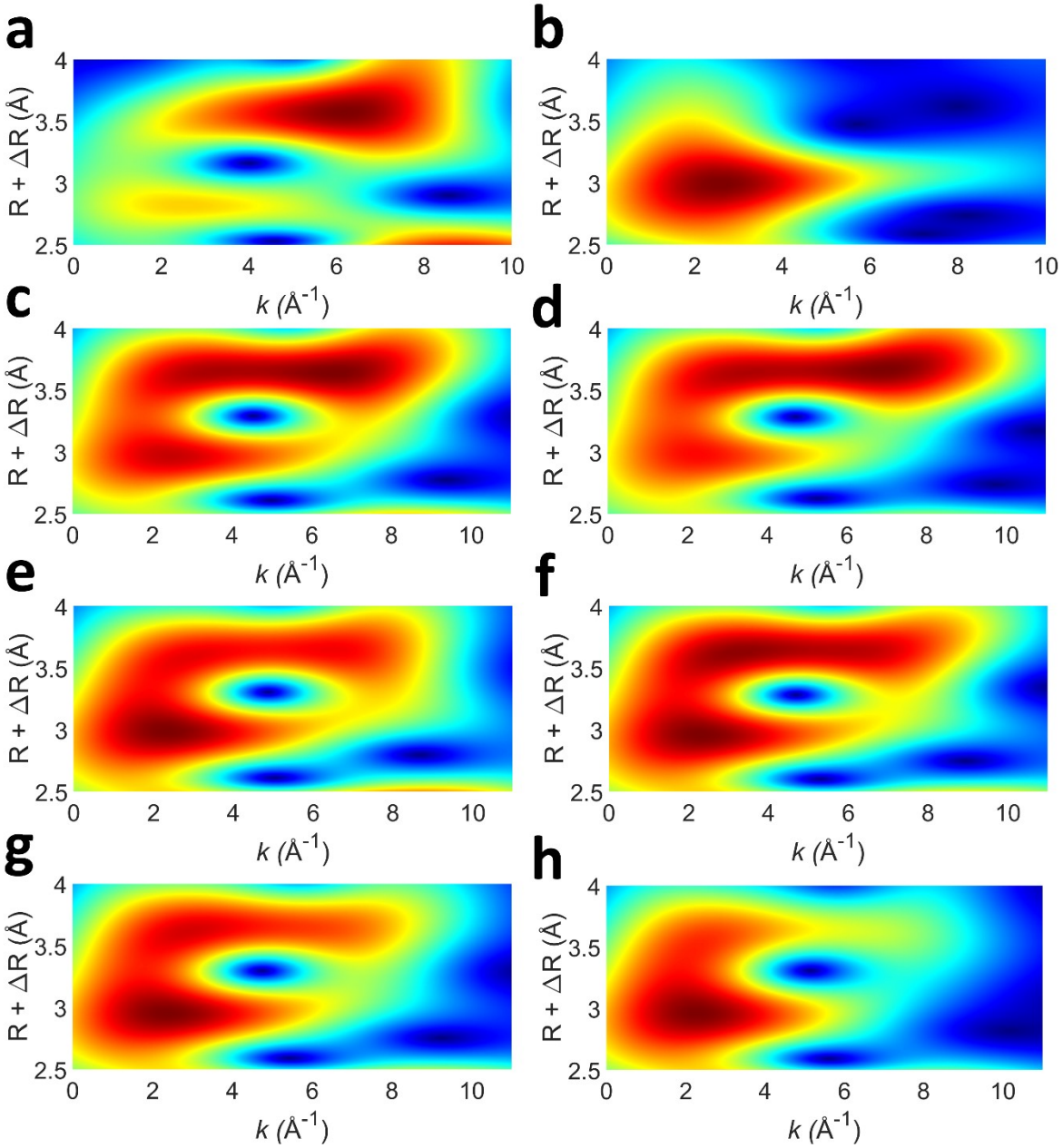

Figure S15: U-L_3 Edge EXAFS wavelet transformation analysis (2.5-4 Å and k_2= 0-10) for (a) UO_2CO_3 standard (b) $UO_2(NO_3)_2$ standard (c) MgAl (d) MgAlFe (e) MgAlCe (f) MgAlNd (g) MgAlEu (h) MgAlTb

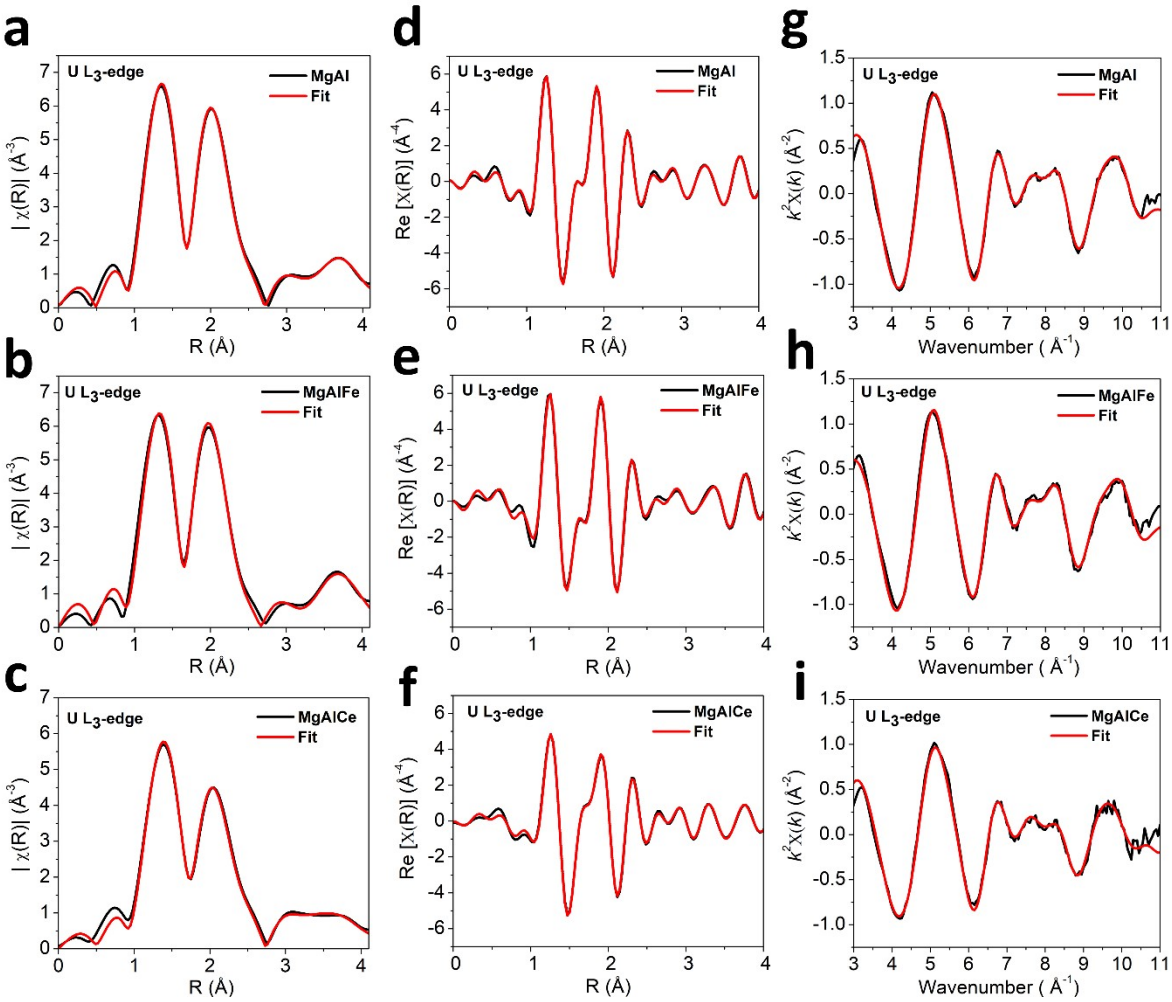

Figure S16: EXAFS spectra and best fit for MgAl, MgAlFe and MgAlCe respectively in (a, b, c) R-space (d,e,f) real part of Fourier-filtered k-space (g,h,i) k space (k_2-weighting)

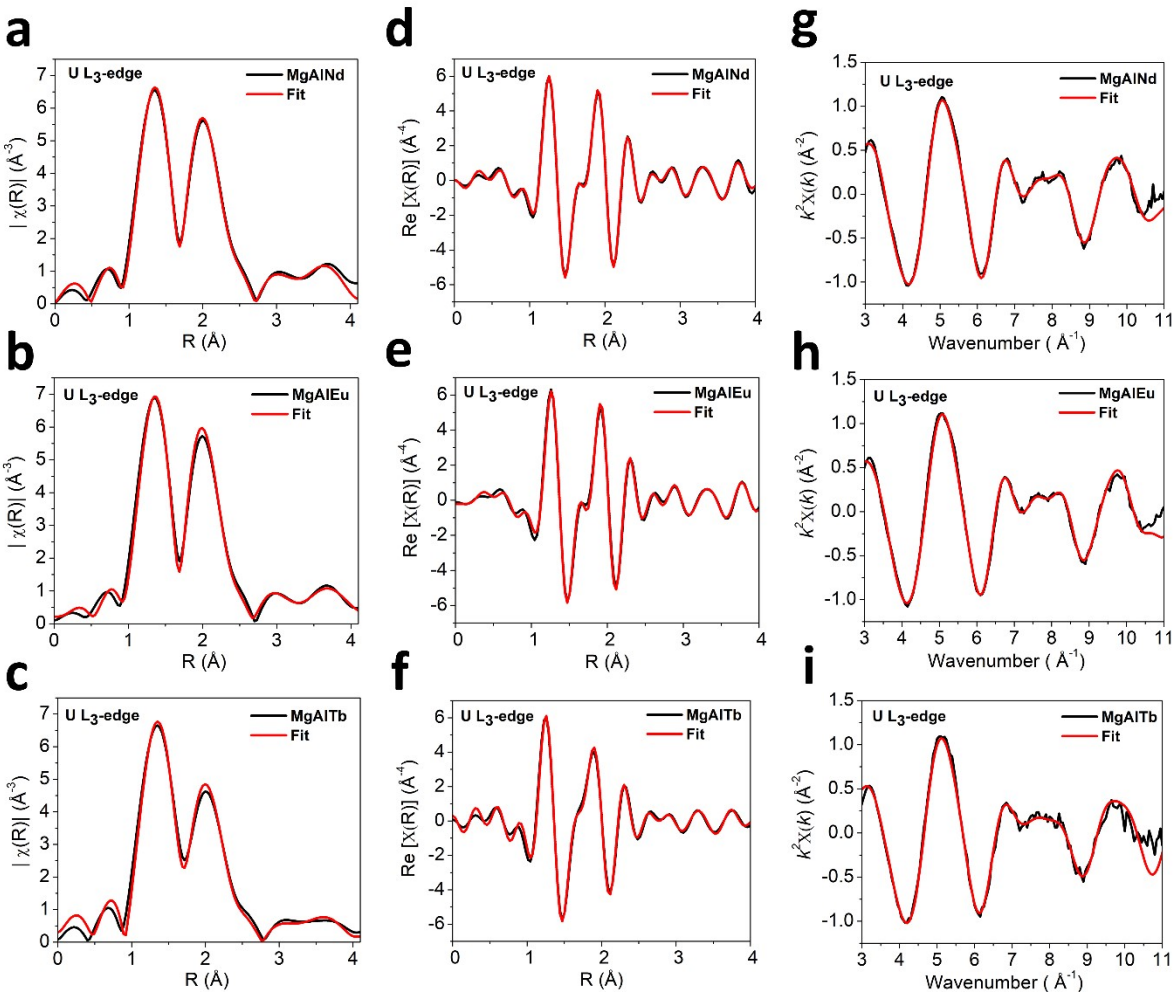

Figure S17: EXAFS spectra and best fit for MgAlNd, MgAlEu and MgAlTb respectively in (a, b, c) R-space (d,e,f) real part of Fourier-filtered k-space (g,h,i) k space (k_2-weighting)

Table S6: EXAFS fitting parameters for U-adsorbed LDH samples

Shell	CN	R (Å)	$\sigma^2 x10^3$ (Å^2)	R-factor
MgAl				
U-O_{ax}	2 $^{\xi}$	1.81 ± 0.007	2.1 ± 0.6	0.0058
U-O_{eq}	4.40 ± 0.38	2.44 ± 0.008	2.1 *	
U-C	2.66 ± 0.6	2.93 ± 0.013	2.1*	
U-U	1.49 ± 0.45	3.48 ± 0.041	2.1 ± 1.8	
U-Mg/Al	5.59 ± 1.2	3.93 ± 0.036	2.1 *	
MgAlFe				
U-O_{ax}	2 $^{\xi}$	1.80 ± 0.008	2.5 ± 0.6	0.0064
U-O_{eq}	4.83± 0.43	2.43 ± 0.009	2.5*	
U-C	2.84 ± 0.74	2.93 ± 0.019	2.5*	
U-U	1.42± 0.51	3.49 ± 0.04	3 ± 0.8	
U-Mg/Al	5.64 ± 1.5	3.94 ± 0.03	3*	
MgAlCe				
U-O_{ax}	2 $^{\xi}$	1.83 ± 0.007	3.1 ± 0.6	0.0058
U-O_{eq}	3.73 ± 0.35	2.46 ± 0.009	3.1*	
U-C	2.56 ± 0.60	2.95 ± 0.018	3.1*	
U-U	1.80 ± 0.56	3.50 ± 0.032	3.2 ± 0.8	
U-Mg/Al	5.08 ± 1.4	3.96 ± 0.035	3.2*	
MgAlNd				
U-O_{ax}	2 $^{\xi}$	1.81± 0.007	2 ± 0.6	0.0061
U-O_{eq}	4.24 ± 0.37	2.44 ± 0.008	2*	
U-C	2.30 ± 0.64	2.93 ± 0.02	2*	
U-U	1.50 ± 0.53	3.48 ± 0.042	3.3 ± 0.9	
U-Mg/Al	5.19 ± 1.42	3.94 ± 0.03	3.3	
MgAlEu				
U-O_{ax}	2 $^{\xi}$	1.81 ± 0.007	1.4 ± 0.6	0.006
U-O_{eq}	4.05 ± 0.36	2.43 ± 0.009	1.4*	
U-C	1.90 ± 0.51	2.94 ± 0.02	1.4*	
U-U	1.13 ± 0.36	3.50 ± 0.06	3.8 ± 0.9	
U-Mg/Al	4.19 ± 1.31	3.95 ± 0.05	3.8*	
MgAlTb				
U-O_{ax}	2 $^{\xi}$	1.81 ± 0.01	1.6 ± 0.9	0.014
U-O_{eq}	3.60 ± 0.5	2.43 ± 0.01	1.6*	
U-C	1.82 ± 0.6	2.95 ±0.04	1.6*	
U-U	1.27 ± 0.4	3.53 ± 0.06	3.9 ± 1.1	
U-Mg/Al	3.21 ± 1.1	3.97 ± 0.07	3.9*	

$^{\xi}$ fixed

* Correlated to same value

Near Edge X-ray Absorption Fine Structure

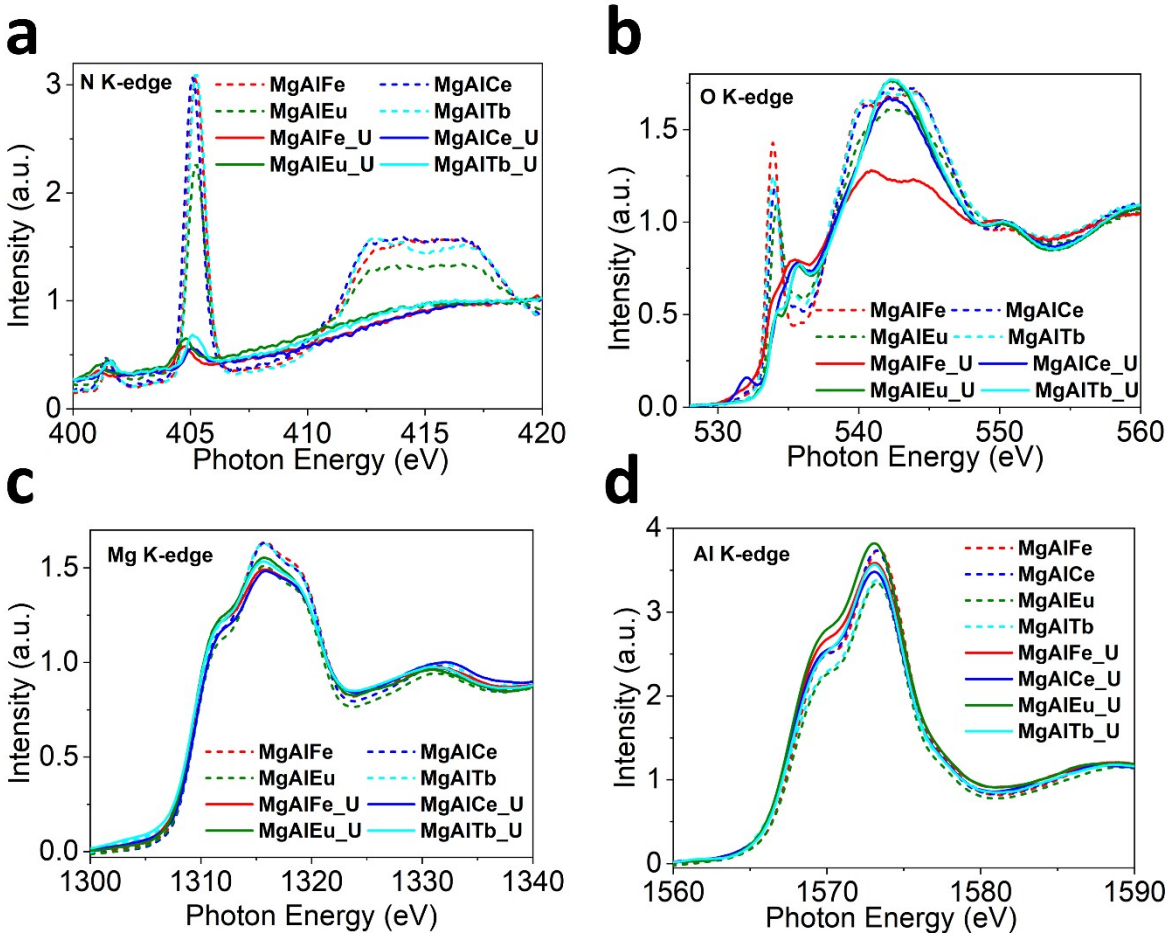

Figure S18: Normalized NEXAFS for (a) Mg K-edge (b) Al K-edge (c) O K-edge and (d) N K-edge (Dash lines represent before adsorption while solid lines depict after adsorption NEXAFS measurements)

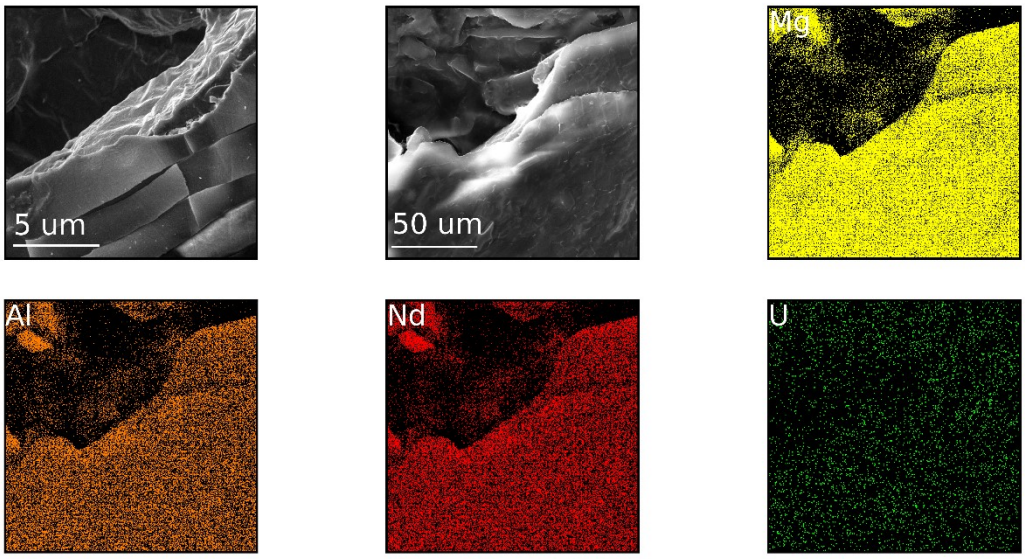

Figure S19: SEM image and EDS maps of MgAlNd after U loading

References

1. Trivedi, M. K. & Dahryn Trivedi, A. B. Spectroscopic Characterization of Disodium Hydrogen Orthophosphate and Sodium Nitrate after Biofield Treatment. *J Chromatogr Sep Tech* **06**, (2015).

2. Ravuru, S. S., Jana, A. & De, S. Synthesis of NiAl- layered double hydroxide with nitrate intercalation: Application in cyanide removal from steel industry effluent. *J Hazard Mater* **373**, 791–800 (2019).

3. Asiabi, H., Yamini, Y. & Shamsayei, M. Highly efficient capture and recovery of uranium by reusable layered double hydroxide intercalated with 2-mercaptoethanesulfonate. *Chemical Engineering Journal* **337**, 609–615 (2018).

4. Hu, Z., Song, X., Wei, C. & Liu, J. Behavior and mechanisms for sorptive removal of perfluorooctane sulfonate by layered double hydroxides. *Chemosphere* **187**, 196–205 (2017).

5. Benhiti, R. *et al.* Synthesis, characterization, and comparative study of MgAl-LDHs prepared by standard coprecipitation and urea hydrolysis methods for phosphate removal. *Environ Sci Pollut Res Int* **27**, 45767–45774 (2020).

6. Zou, Y. *et al.* Controllable Synthesis of Ca-Mg-Al Layered Double Hydroxides and Calcined Layered Double Oxides for the Efficient Removal of U(VI) from Wastewater Solutions. *ACS Sustain Chem Eng* **5**, 1173–1185 (2017).

7. Sing, K. S. W. *et al.* Reporting Physisorption Data for Gas/Solid Systems with Special Reference to the Determination of Surface Area and Porosity. *Pure and Applied Chemistry* **57**, 603–619 (1985).

8. Muñoz, M., Farges, F. & Argoul, P. Continuous Cauchy wavelet transform of XAFS spectra. *Physica Scripta T* **T115**, 221–222 (2005).

9. Chui, C. K. *Introduction to Wavelets.* (Academic Press, 1992).